Saudi Pharmaceutical Journal 32 (2024) 102064

HOSTED BY

Contents lists available at ScienceDirect

Saudi Pharmaceutical Journal

journal homepage: www.sciencedirect.com

Original article

Sorafenib and Piperine co-loaded PLGA nanoparticles: Development, characterization, and anti-cancer activity against hepatocellular carcinoma cell line

Sulaiman S. Alhudaithi [a,*], Mohd Abul Kalam [a], Lama Binobaid [b], Raisuddin Ali [a], Mohammed M. Almutairi [b], Wajhul Qamar [b], Hessa Bin Hithlayn [a], Atheer Almutairi [a], Abdullah K. Alshememry [a]

[a] Department of Pharmaceutics, College of Pharmacy, King Saud University, P.O. Box 2457, Riyadh 11451, Saudi Arabia
[b] Department of Pharmacology and Toxicology, College of Pharmacy, King Saud University, P.O. Box 2457, Riyadh 11451, Saudi Arabia

ARTICLE INFO

Keywords:
Hepatocellular carcinoma
Sorafenib
Piperine
Poly (lactic-co-glycolic acid)
Emulsification-solvent-evaporation

ABSTRACT

Hepatocellular carcinoma (HCC) exhibits high mortality rates in the advanced stage (>90 %). Sorafenib (SORA) is a targeted therapy approved for the treatment of advanced HCC; however, the reported response rate to such a therapeutic is suboptimal (<3%). Piperine (PIP) is an alkaloid demonstrated to exert a direct tumoricidal activity in HCC and improve the pharmacokinetic profiles of anticancer drugs including SORA. In this study, we developed a strategy to improve efficacy outcomes in HCC using PIP as an add-on treatment to support the first-line therapy SORA using biodegradable Poly (D, L-Lactide-co-glycolide, PLGA) nanoparticles (NPs). SORA and PIP (both exhibit low aqueous solubility) were co-loaded into PLGA NPs (PNPs) and stabilized with various concentrations of polyvinyl alcohol (PVA). The SORA and PIP-loaded PNPs (SP-PNPs) were characterized using Fourier Transform Infrared (FTIR) Spectroscopy, X-ray Powder Diffraction (XRD), Dynamic Light Scattering (DLS), and Scanning Electron Microscopy (SEM), Release of these drugs from SP-PNPs was investigated *in vitro* at both physiological and acidic pH, and kinetic models were employed to assess the mechanism of drug release. The *in vitro* efficacy of SP-PNPs against HCC cells (HepG2) was also evaluated. FTIR and XRD analyses revealed that the drugs encapsulated in PNPs were in an amorphous state, with no observed chemical interactions among the drugs or excipients. Assessment of drug release *in vitro* at pH 5 and 7.4 showed that SORA and PIP loaded in PNPs with 0.5 % PVA were released in a sustained manner, unlike pure drugs, which exhibited relatively fast release. SP-PNPs with 0.5 % PVA were spherical, had an average size of 224 nm, and had a high encapsulation efficiency (SORA ~ 82 %, PIP ~ 79 %), as well as superior cytotoxicity compared to SORA monotherapy *in vitro*. These results suggest that combining PIP with SORA using PNPs may be an effective strategy for the treatment of HCC and may set the stage for a comprehensive *in vivo* study to evaluate the efficacy and safety of this novel formulation using a murine HCC model.

1. Introduction

Hepatocellular carcinoma (HCC) is the most common type of liver cancer and the third main cause of cancer related deaths worldwide (Yang et al., 2023; Zhuo et al., 2019). Up to 75 % of patients who develop HCC have a history of risk factors including chronic liver diseases such as hepatitis and cirrhosis (Gomaa et al., 2008; Yang et al., 2019). Despite advancements in HCC treatment in recent decades, survival rates remain poor. The 5-year relative survival rate in the localized stage is < 40 %, whereas in the distant stage, it is lower than 4 % (Neureiter et al., 2019; Siegel et al., 2019).

Sorafenib (SORA) is a multi-target tyrosine kinase inhibitor currently used as a first-line treatment in unresectable and metastatic HCC (Furuse, 2008; Laface et al., 2022; Nguyen et al., 2023). SORA is highly hydrophobic with a reported 38 to 49 % bioavailability of its salt form (SORA Tosylate) (Liu et al., 2016). Due to its low pharmacokinetic profile, it is administered twice daily to HCC patients at a high dose (400 mg) (Ben Mousa, 2008). Despite being a drug of choice, the phase III

* Corresponding author.
E-mail address: salhudaithi@ksu.edu.sa (S.S. Alhudaithi).

https://doi.org/10.1016/j.jsps.2024.102064
Received 18 January 2024; Accepted 6 April 2024
Available online 7 April 2024

clinical trial (SHARP) that led to SORA FDA approval revealed that the overall response rate to SORA in HCC patients is suboptimal (2 %), with only slight improvement in overall survival compared to placebo (2.8 months median improvement) (Storandt et al., 2022). However, no other targeted therapies tested in phase III clinical studies showed superiority to SORA in terms of HCC survival rates (Colagrande et al., 2016; Zhang et al., 2023).

Plant-derived natural products, such as flavonoids and alkaloids have been extensively investigated in preclinical studies for the treatment of several cancers, including breast, lung, and liver cancer (Kopustinskiene et al., 2020; Li et al., 2022). Piperine (PIP), an alkaloid constituent of black pepper, has been shown to exhibit antitumor, hepatoprotective, antihypertensive, antioxidant, and antimicrobial activities when used as monotherapy or in combination with other bioactive plant extracts and with standard anticancer therapies (Tripathi et al., 2022). PIP is also a bioenhancer; it inhibits P-glycoprotein (Pgp), a major drug transporter largely involved in the efflux of several anticancer drugs including tyrosine kinase inhibitors, which may potentially lead to drug resistance (Finch and Pillans, 2014; Syed et al., 2017; Tripathi et al., 2022). Moreover, PIP has been shown to inhibit CYP3A4, a major drug-metabolizing enzyme (Wang et al., 2013). Inhibition of Pgp and CYP3A4 is strongly associated with the enhancement of absorption and bioavailability of many drugs including anticancer drugs (Gao and Hu, 2010). The bioavailability of curcumin was enhanced by 1.5 times in rats and 20 times in human volunteers when administered with PIP (Shoba et al., 1998). PIP has also been shown to improve the pharmacokinetic properties of SORA, which was likely attributed to its Pgp and/or CYP3A4 inhibitory effect (Patel et al., 2022; Tiwari et al., 2020; Tiwari et al., 2021).

Given the prominent role of PIP in cancer and the suboptimal effect of SORA in the treatment of HCC, we set out to investigate whether the incorporation of PIP as an add-on to the standard-of-care therapy SORA would lead to superior anticancer effects against HCC compared to SORA treatment alone. Our novel strategy aimed to encapsulate SORA and PIP (both highly lipophilic molecules) in Poly Lactic-co-Glycolic Acid (PLGA) based nanoparticles (NPs) and examine the impact of the therapeutic on HCC. PLGA, a biodegradable and biocompatible polymer (Lu et al., 2023; Rocha et al., 2022), is FDA-approved and widely been employed in drug delivery applications (Alsaab et al., 2022; Makadia and Siegel, 2011). Many reports have revealed that PLGA-based NPs (PNPs), when used as drug carriers, can prolong the release of drugs, potentially reducing the dosing frequency, minimizing off-target side effects of therapeutics, and increasing drug stability (Alvi et al., 2022; Bai et al., 2022; Shao et al., 2022). PLGA has also been shown to be an optimal vehicle for a variety of hydrophobic compounds as it enhances their aqueous solubility, and thereby, their efficacy (Caputo et al., 2023; Makadia and Siegel, 2011).

This work involves development of dual drug-loaded PNPs and their associated characterization, drug release studies, as well as the assessment of the therapeutic efficacy on HCC cells (HepG2) using *in vitro* techniques.

2. Materials and methods

2.1. Materials

HepG2 cells were purchased from the American Type Culture Collection (ATCC®). Dulbecco's modified Eagle's medium (DMEM), high glucose with sodium pyruvate (Gibco™), fetal bovine serum (FBS, Gibco™), and penicillin–streptomycin antibiotics 100x (Capricorn™) were obtained from ThermoFisher (Massachusetts, USA). SORA ($C_{21}H_{16}ClF_3N_4O_3$; Mw 464.825 g/mol) was purchased from LC Laboratories®, MA, USA. PIP ($C_{17}H_{19}NO_3$; Mw 285.35 g/mol) and the Annexin V-FITC/PI Apoptosis Detection-Kit (catalog # HY-K1073) were obtained from MedChemExpress LLC, NJ, USA. Poly (D, L-lactic-co-glycolic acid; 50: 50) with 40,000–75,000 Mw, polyvinyl alcohol (PVA) with 30,000 Mw, acetone, dimethyl sulfoxide (DMSO), ethanol, Kolliphor® EL, and Thiazolyl Blue Tetrazolium Bromide (MTT) (catalog # M2128) were provided by Sigma Aldrich Co. (St. Louis, MO, USA). Tween-80 was supplied by Eurostar Scientific Ltd. Liverpool, UK. Acetonitrile, methanol (HPLC grades), and formic acid were obtained from "BDH Ltd. (Poole, England)". Phosphate buffered saline (PBS) was purchased from Life Technologies™ (Frederick, MD, USA). Dialysis membrane with a molecular weight cutoff of 12–14 kDa was supplied by Spectra/Por®, Spectrum Lab Inc., (Rancho Dominguez, CA, USA). Milli-Q water was obtained from Millipore filter unit (Millipore, Molsheim, France). All chemicals used were of analytical grade.

2.2. High-performance liquid chromatography (HPLC) analysis of SORA and PIP

A previously reported HPLC with UV-detection was utilized for the simultaneous quantification of SORA and PIP (Escudero-Ortiz et al., 2015; Tiwari et al., 2020). A reversed-phase C_{18} column (SunFire™ columns by Waters®, 5 µm, 4.6 × 250 mm) was connected to a Waters® HPLC system (1500-series controller, Milford, MA, USA). Other essential HPLC parts were used, including binary pump (Model-1525), autosampler (Model-2707), and dual absorbance UV-detector (Model-2489). The system was controlled and monitored by Breeze 2 software for data collection and calculations, and the column was maintained at 25 °C. The mobile phase consisted of acetonitrile (70 % v/v) and water with formic acid (29.5 %: 0.5 %, v/v). The mobile phase components were filtered through a 250-µm membrane filter and sonicated for 20 min for degassing. Subsequently, the mobile phase compositions were pumped isocratically to the HPLC system at 1 mL/min of flow rate. Simultaneous detection of both drugs was performed at 280 nm UV-detection (isosbestic point for SORA and PIP) (Tiwari et al., 2020). The injection volume was 30 µL and the total run-time was 10 min.

The stock solution of the drug mixture was prepared by dissolving 10 mg of each drug in 100 mL of acetonitrile (100 µg/mL). Standard calibration of samples was prepared by diluting the stock solution. The mobile phase mixture was used for further dilutions to obtain a concentration range of 0.25–50 µg/mL for each drug.

2.3. Preparation of PLGA NPs

PNPs, co-loaded with SORA and PIP (SP-PNPs) were prepared by using the commonly employed "emulsification solvent evaporation method" as described in previous reports (Caputo et al., 2023; Kalam and Alshamsan, 2017; Rezvantalab et al., 2018; Song et al., 2008). Briefly, 60 mg of PLGA, 4.5 mg of SORA and 2.5 mg of PIP were dissolved in 2.5 mL of acetone (organic phase). PVA was dissolved in Milli-Q water at 0.25, 0.5, or 1 %, w/v concentration (aqueous phase). The organic phase was gradually added drop by drop to 7.5 mL of the aqueous phase under magnetic stirring (750 rpm) and emulsified by probe sonication (Sonics & Materials, Inc., Newtown, CT, USA) at 40 W power in an ice-bath for 1 min followed by homogenization at 21,500 rpm for 5 min (IKA®-WERKE, GMBH & Co., Staufen, Germany) to form the primary emulsion. After the primary emulsion was prepared, additional aqueous phase (three times the volume of the primary emulsion) was added with magnetic stirring to facilitate the formation of droplets. The organic solvent was allowed to evaporate by magnetic stirring for 4 h at room temperature, resulting in PNPs suspended in the aqueous phase. the suspended PNPs were then purified by multiple washes with Milli-Q water for purification by ultracentrifugation at 4 °C for 30 min at 30,000 rpm (Preparative Ultracentrifuge, WX-series, Hitachi Koki, Ibaraki, Japan). The supernatant was discarded and the pellet of PNPs was freeze-dried at 0.02 mbar and −50 °C for 24 h (FreeZone-4.5 Freeze Dry System, Labconco Corporation, Kansas, MO, USA) for subsequent studies. PNPs loaded with SORA (S-PNPs), PIP (P-PNPs) and blank PNPs (B-PNPs) were prepared in a similar fashion. Pure drug solutions of SORA and PIP (SP-SOL) were prepared by dissolving appropriate

amounts of the drugs in a 3:1 (v/v) mixture of ethanol and Kolliphor® EL for comparative *in vitro* release profiling (Yang et al., 2016). All batches of formulations were prepared in triplicate.

2.4. Particle size, polydispersity index (PDI) and zeta potential (ζ) measurements

The average size and PDI of the developed PNPs were determined by dynamic light scattering (DLS) measurement using Zetasizer Nano ZS90 (Malvern Instruments Ltd., Malvern, UK) at 25 °C and a 90° scattering angle for optimal detection. The PNP suspensions were diluted with Milli-Q water (1:10) before each measurement. The PDI ranged from 0 to 1. The ζ of the PNPs was determined by DLS at 25 °C using the same aqueous dilution. Water was selected as diluent due to its dielectric constant value of ~ 78. The Zetasizer was equipped with DTS version 4.1 (Malvern, England) software capable of measuring the electrophoretic mobility of the suspended NPs, which was then converted to a numerical value of ζ (mV) by the software. Measurements were performed in triplicate for each formulation.

2.5. Scanning electron microscope (SEM) imaging

SEM (Zeiss EVO LS10, Cambridge, UK) imaging was performed using the standard gold-sputter technique to assess the morphology of the developed PNPs. The PNP samples were coated with gold using an "Ion-Sputter" for 60 sec at 20 mA current. Scanning was performed at an accelerating voltage of 20 kV, with a working distance of 7.5–9.0 mm, and magnification of 25,000 to 40,000 times.

2.6. Drug encapsulation and loading efficiencies

Drug encapsulation and loading efficiencies were calculated by indirect method, where the unencapsulated drugs were measured. Following purification by ultracentrifugation, the pellet of SORA and PIP-loaded PNPs was resuspended with 5 mL of Milli-Q water. Subsequently, 1 mL of PNPs suspension was centrifuged again for 30 min, and the supernatant was collected. A 30 µL aliquot of the supernatant was then injected into the HPLC system for the quantification of the unentrapped SORA and PIP in the PNPs. The chromatographic separation of the two drugs was achieved using the adopted HPLC-UV method at the isosbestic point of both drugs (280 nm), as mentioned above. The experiment was performed in triplicate. Encapsulation efficiency (%EE) and loading capacity (%DL) were calculated by the following equations (Eq. 1 and Eq. (2):

$$\%EE = \left(\frac{Initialamountofdrug(\mu g) - Finalamountofdrug(\mu g)}{Initialamountofdrug(\mu g)}\right) \times 100 \ldots. \quad (1)$$

$$\%DL = \left(\frac{Initialamountofdrug(\mu g) - Finalamountofdrug(\mu g)}{TotalamountofPNPs(\mu g)}\right) \times 100 \cdots \quad (2)$$

2.7. Fourier Transform infrared (FTIR) spectroscopy

FTIR was performed for the pure drugs (SORA and PIP), PLGA, the physical mixture of drugs and PLGA, freeze-dried B-PNPs, and SP-PNPs using BRUKER Optik GmBH (Model ALPHA, Germany). Approximately 5 mg of each sample was placed on a holder plate and exposed to a range of infrared spectra. The instrument was equipped with OPUS software version 7.8. The spectra of all samples were recorded from 4000 to 400 cm^{-1} wavenumber at 2 cm^{-1} resolution.

2.8. X-ray Powder diffraction (XRD)

Samples were ground using a mortar and pestle. XRD analysis of the pure drugs (SORA and PIP), PLGA, the physical mixture of drugs and PLGA, freeze-dried B-PNPs, and SP-PNPs was performed using "Ultima-IV Diffractometer (Rigaku, Inc. Japan)" at 2-theta (2θ°) over a range of 3 to 100° and a scan speed of 1 deg/min. The X-ray tube was composed of copper (Cu) as the anode material with Kα2 elimination (λ) of 0.154 nm and was monochromatized with a graphite crystal. The diffraction pattern was recorded at 40 kV voltage and 40 mA current for the generator in step scan mode. The step size was 0.02° and counting time was 1 sec per step.

2.9. In vitro release of SORA and PIP from SP-PNPs

In vitro release profiles of SORA and PIP were assessed in PBS release medium at two pH conditions, neutral (pH 7.4) and acidic (pH 5), which are representative of the physiological and the tumor microenvironment pH, respectively (Ebadi et al., 2020). Tween-80 (0.5 %) was added to the release media to enhance the solubilization of the highly lipophilic drugs. For comparative release profiling, SORA and PIP solutions (SP-SOLs) were prepared by dissolving the same drug quantities as in PNPs in a 3:1 (v/v) mixture of ethanol and Kolliphor® EL (Yang et al., 2016). One milliliter of each SP-PNP suspension and SP-SOLs was placed into activated 12 kDa MWCO dialysis bags (Spectra/Por® Standard RC Tubing). Both ends of the bags were securely sealed by appropriate closures and they were immersed in 50 mL of release media using beakers. Three sets of beakers for each formulation were placed into a shaking water bath and maintained at a speed of 100 S/min and a temperature of 37 ± 2 °C. Samples (1 mL) were collected from each beaker at various time points to assess the release of drugs. To maintain sink conditions, 1 mL of fresh release medium (kept at 37 ± 2 °C) was added to the beakers after each sampling. The collected samples were transferred to HPLC vials and 30 µL of each sample was injected into an HPLC-UV system for the simultaneous quantification of SORA and PIP at 280 nm (Tiwari et al., 2020). The percentage of drug released (%DR) was estimated using **Eq. 3**. Thereafter, the %DR was plotted against time (h) to obtain the release profiles of both drugs.

$$\%DR = \frac{Conc.(\mu g/mL) \times DF \times Volumeofreleasemedium(mL)}{Initialamountofdrugused(\mu g)} \times 100 \ldots\ldots (3).$$

2.10. Release kinetics of SORA and PIP from SP-PNPs

The release kinetics of SORA and PIP in SP-PNP formulations were determined by fitting the *in vitro* release data to different kinetic equations (release models). The models utilized in this investigation were zero-order, first-order, Korsmeyer-Peppas, Higuchi-matrix (square root model), and Hixson-Crowell models. Among the applied models, the one that showed the highest value of correlation-coefficient (R^2) was considered the best-fit model for drug release. By using the slopes of the regression equations, obtained from the plots, the release-exponent (*n*-values) was calculated to examine the mechanism of drug release from SP-PNPs. In addition, the *K*-values (the release constant) for all models were estimated.

2.11. Cell culture

Human hepatocellular carcinoma cells (HepG2) were grown in a complete medium composed of DMEM supplemented with 10 % FBS and 1 % penicillin–streptomycin antibiotics and maintained in culture at 37 °C and 5 % CO2.

2.12. In vitro anticancer activity

2.12.1. Cell proliferation (MTT assay)

The anti-proliferative effect of SP-PNPs, pure SORA, and pure PIP on HepG2 cells was assessed using MTT assay. The pure drugs were solubilized in a solution composed of DMSO and Tween-80 in deionized water, and then diluted in cell culture media (0.003 % DMSO and 0.03 % Tween 80). Seven thousands cells were plated in 96-well plates and cultured in complete media at 37 °C and 5 % CO2 for 24 h. Cells were

then treated for 72 h with various concentrations of SORA (0.94–15 μg/mL), PIP (0.94– 15 μg/mL), a mixture of the pure drugs (0.94/0.47 – 15/7.5 μg/mL), and SP-PNPs (equivalent to 0.94/0.47 – 15/7.5 μg/mL, SORA/PIP), as well as equivalent amounts of drug-free NPs or B-PNPs using 3 % FBS containing-DMEM cell culture media. Thereafter, the MTT assay was performed as follows; 15 μL of 5 mg/mL MTT stock solution (dissolved in 1x PBS) was added to each well. The cells were then undergone shaking for 5 min before incubating at 37 °C and 5 % CO_2 for 2 h in the dark. After that, the medium was completely removed from the wells and replaced with 200 μL of isopropyl alcohol to solubilize formazan. Cells were then mixed by shaking for 10 min before the absorbance was measured at 570 nm using microplate reader (Synergy HT, BioTek®). The "cells only" group was used as the control, with their average absorbance representing 100 % cell viability. The average absorbance of the "positive control" group (cells treated with 5 % DMSO) was considered 0 % viability, and the percentage viabilities in all groups were estimated with respect to controls readings (0 and 100 %). To calculate IC_{50} values and the confidence interval (CI) for the various treatment groups, nonlinear fit of normalized data (log inhibitor *vs.* normalized response) was used.

2.12.2. Apoptosis/Necrosis assay

To further evaluate the cytotoxic effect of SP-PNPs on HepG2 cells and determine the mechanism of cell kill, an apoptosis/necrosis assay was performed. Briefly, 1 x 10^5 cells were plated in 6-well plates and cultured in complete media at 37 °C and 5 % CO2 for 24 h. Cells were then treated for 72 h with 2 μg/mL of SORA, 1 μg/mL of PIP, SP-PNPs containing 2 μg/mL of SORA with 1 μg/mL of PIP, and B-PNPs (with equivalent polymer concentrations as in SP-PNPs). Following treatment, the cells were trypsinized, washed with 1x PBS and re-suspended in binding buffer prior to being stained with 5 μL of Annexin and 10 μL of PI. The cells were then incubated in the dark at room temperature for 20 min. After that, Flow-cytometric analysis was performed using a Beckman Coulter Flow-cytometer (Indianapolis, IN, USA). Cells undergone only necrosis were identified as PI^+, the $Annexin^+$ cell population is representative of early apoptosis, and the PI^+ $Annexin^+$ population represented late apoptotic cells.

2.13. Statistical analysis

Data are presented as means with standard deviations (Mean ± SD) or standard error of the mean (±SEM). Statistical analyses were performed using GraphPad Prism: Versions 5.1 and 8.0.1 (GraphPad Software, Inc., San Diego, CA, USA). One-way ANOVA and Kruskal-Wallis tests were used to compare between treatment groups and the control in the efficacy experiments, and statistical significance was considered when *p*-values were less than 0.05 ($p < 0.05$). ROUT analysis was used to eliminate outliers in the efficacy experiments.

3. Results

3.1. HPLC analysis of SORA and PIP at isosbestic point

The HPLC method used (Tiwari et al., 2020) was deemed appropriate for chromatographic separation and simultaneous quantification of SORA and PIP. Calibration curves for both drugs were linear within the specified concentration range (0.25–50 μg/mL). The regression equations for SORA and PIP had correlation coefficients (R^2) of 0.9979 and 0.9994, respectively. Moreover, the retention times for SORA and PIP were 6.29 min and 4.98 min, respectively.

3.2. Development of SP-PNPs and initial characterization

Particle size, PDI, and ζ of the various prepared PNPs are listed in Table 1**.** The developed PNPs were ranged in size from 221 to 420 nm. The ζ measurements for all the prepared formulations, including B-PNPs, had negative values of low magnitude (−3.7 and −7.4). Among the developed formulations (Table 1), PNPs with 0.5 % PVA exhibited the least PDI, indicating superior homogeneity.

Table 1
Physical characterization of the developed PNPs. Data are presented as the averages of at least three measurements with standard deviations (Mean ± SD, $n \geq 3$).

PLGA-NPs	Parameters		
	Particle size (nm)	Polydispersity index (PDI)	Zeta potential (ζ) (mV)
SP-PNPs (0.25 %, PVA)	221.21 ± 15.74	0.246 ± 0.060	−3.73 ± 1.85
SP-PNPs (0.5 %, PVA)	224.82 ± 14.04	0.131 ± 0.068	−5.01 ± 1.78
SP-PNPs (1 %, PVA)	420.56 ± 26.22	0.592 ± 0.244	−7.38 ± 1.67
B-PNPs (0.5 %, PVA)	202.16 ± 18.98	0.192 ± 0.092	−5.85 ± 2.35

SP-PNPs: Sorafenib-Piperine co-encapsulated PLGA-NPs; B-PNPs: Blank PLGA-NP.

3.3. Encapsulation and drug loading

The %EE and %DL of both drugs are listed in Table 2. Similar to the effect on the size of polymeric NPs, the drug-to-polymer ratio significantly influences the encapsulation of drugs into NP cores. A drug-to-polymer ratio of approximately 1:9 (w/w) drugs (SORA and PIP) to PLGA was used to prepare SP-PNPs. The results (Table 2) showed that PNPs were more efficient in loading SORA compared to PIP (SORA: > 6.5 %DL, PIP: < 3.5 %DL). The entrapment of SORA and PIP in 0.5 % PVA PNPs resulted in higher %EE (82.13 % and 78,93 %, respectively) compared to PNPs with 0.25 % and 1 % PVA. However, PVA concentration did not have a significant impact on drug entrapment for either drug, which is different than its effect on PNP size and ζ (as described in Section 3.2). Therefore, based on these findings, 0.5 % (w/v) was chosen as the optimal concentration of PVA for preparing SP-PNPs for *in vitro* drug release and efficacy studies.

3.4. SEM analysis

The shape and surface structures of PNPs, prepared with various PVA concentrations were evaluated by SEM using magnifications ranging from 25,000 to 40,000 times, as depicted in Fig. 1. SEM imaging revealed that the developed PNPs had fairly regular and spherical solid dense structures with smooth surfaces and without overt aggregation. No noticeable differences were observed in the surface morphology between B-PNPs and SP-PNPs.

3.5. FTIR spectroscopy

FTIR is a commonly used technique for obtaining material- specific

Table 2
%EE and %DL of the developed SP-PNPs. Data are represented as the averages of three measurements with standard deviations (Mean ± SD, $n = 3$).

PLGA-NPs	%EE		%DL	
	SORA	PIP	SORA	PIP
SP-PNPs (0.25 %, PVA)	78.92 ± 3.98	73.10 ± 4.44	6.86 ± 0.34	3.18 ± 0.19
SP-PNPs (0.5 %, PVA)	82.13 ± 5.97	78.93 ± 7.18	7.14 ± 0.52	3.43 ± 0.31
SP-PNPs (1 %, PVA)	77.72 ± 3.19	76.58 ± 4.13	6.76 ± 0.28	3.32 ± 0.18

SP-PNPs: Sorafenib-Piperine co-encapsulated PLGA-NPs; SORA: Sorafenib and PIP: Piperine.

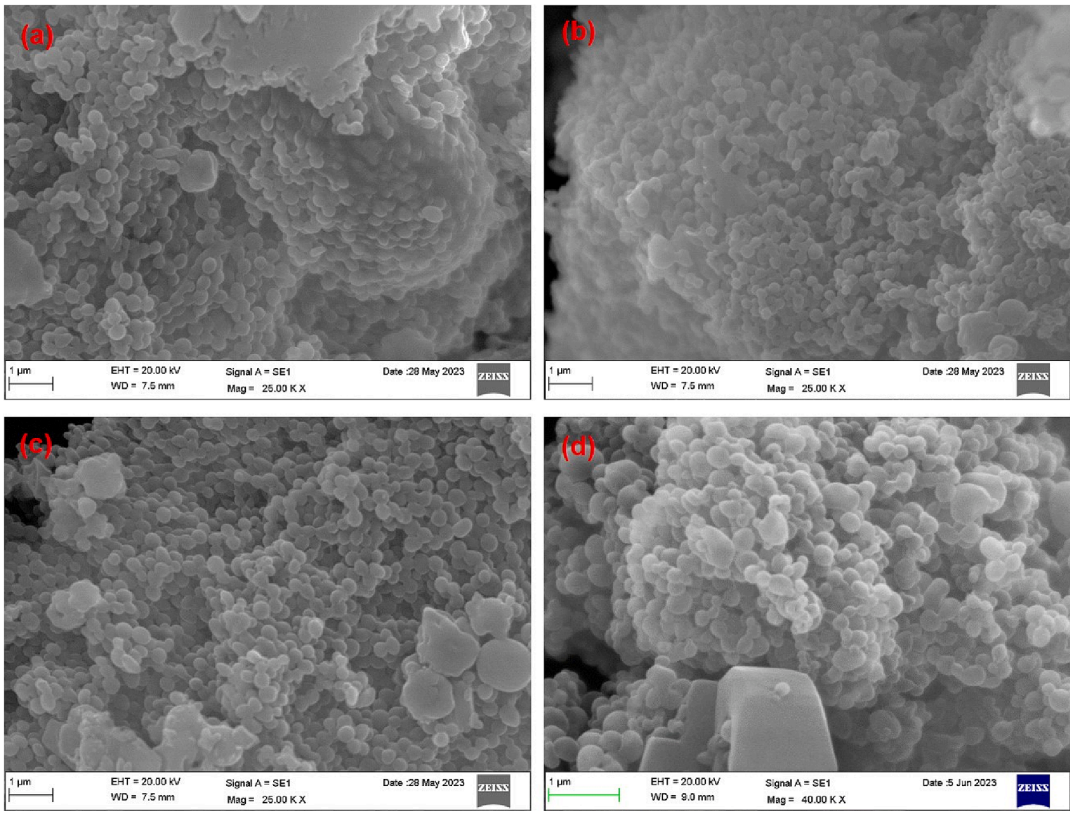

Fig. 1. Scanning electron micrographs of PNPs, prepared with different concentrations of polyvinyl alcohol (PVA): 0.25% PVA SP-PNPs **(a)**; 0.5% PVA B-PNPs **(b)**; 0.5% PVA SP-PNPs **(c)**; 1% PVA SP-PNPs **(d).**

IR spectra, and it is useful for identifying potential interactions among molecules. FTIR analysis is fast, sensitive, and precise compared to other IR methods, making it an ideal method for analysing small samples (Eid, 2022). In this study, IR spectra of the pure drugs (SORA and PIP), PLGA, the physical mixture of SORA, PIP, and PLGA, freeze-dried B-PNPs, and SP-PNPs were generated as shown in Fig. 2**.**

The IR spectra of pure SORA (Fig. 2**a**) demonstrated the characteristic bands of C–O stretching (at 1123.10 cm^{-1}), C–NH stretching (1641.13 cm^{-1}), C = O stretching (at 1704.48 cm^{-1}), CH stretching band for aliphatic CH (at 3073.21 cm^{-1}), CH stretching band for aromatic CH (at 3293.67 cm^{-1}), and OH bending (at 3332.29 cm^{-1}) (Caputo et al., 2023; Stăncioiu et al., 2022). The spectra of pure PIP

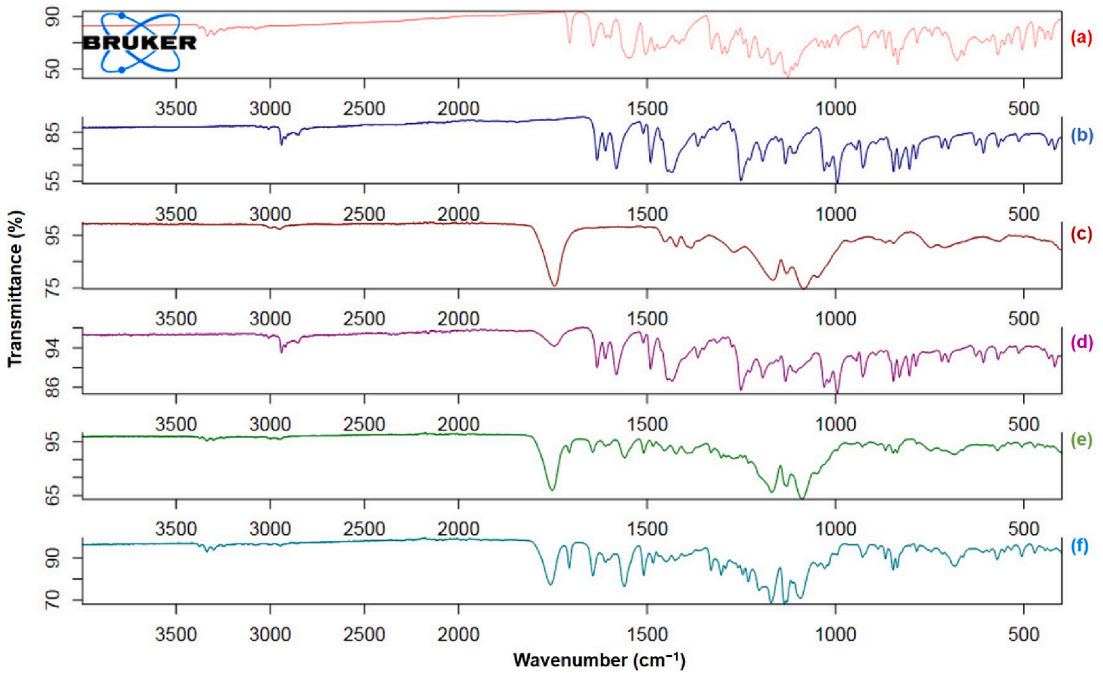

Fig. 2. Overlay infrared spectra of pure-SORA **(a)**; pure-PIP **(b)**; pure-PLGA **(c)**; the physical mixture of drugs and PLGA **(d)**; B-PNPs **(e)**; SP-PNPs **(f)**.

(Fig. 2**b**), showed an out of plane C–H bending (at 837.60 cm^{-1}), C–O stretching (at 925.73 cm^{-1}), C–H stretching, C–H bending of trans –CH = CH– (at 998.77 cm^{-1}), =C–O–C asymmetric stretching (at 1243.48 cm^{-1}), C = C stretching (at 1436.17 cm^{-1}), symmetric and asymmetric stretching of C = O diene (at 1522.45 cm^{-1}), C = O stretching (at 1578.14 cm^{-1}), –CO–N stretching (at 1623.60 cm^{-1}), –NCH_2 stretching (at 2856.57 cm^{-1}), stretching band of aliphatic C–H (at 2931.84 cm^{-1}), and stretching band of aromatic C–H (at 3006.51 cm^{-1}) (Zarai et al., 2013).

The spectra of pure PLGA (Fig. 2**c**) had C–H bending vibrations at 1084.09 cm^{-1}, 1170.09 cm^{-1}, and 1268.39 cm^{-1}. The characteristic band at 1385.87 cm^{-1} was due to the bending vibration of C = O, at 1747.39 cm^{-1} was due to–COO stretching, and at 2951.87 cm^{-1} was due to C–H stretching vibration (Singh et al., 2014). The IR spectra of the physical mixture of drugs and PLGA (Fig. 2**d**) showed mixed bands of different functional groups of SORA, PIP, and PLGA. These bands were observed at 837.73 cm^{-1} for C–H bending (out of plane), 925.84 cm^{-1} (C–O stretching for PIP), 999.12 cm^{-1} (C–H stretching and C–H bending of trans –CH = CH– for PIP), 1120.88 cm^{-1} (C–O stretching), 1191.58 cm^{-1} (C–H bending vibration), 1243.58 cm^{-1} (=C–O–C asymmetric stretching), 1360.19 cm^{-1} (bending vibration of C = O), 1436.16 cm^{-1} (C = C stretching for PIP), 1491.97 cm^{-1} (symmetric and asymmetric stretching of C = O), 1578.21 cm^{-1} (C = O stretching), 1623.57 cm^{-1} (possibly –C–NH stretching for SORA or –CO–N stretching for PIP), 2857.31 cm^{-1} (–NCH_2 stretching), 2931.85 cm^{-1} (stretching band of aliphatic CH) and 3007.15 cm^{-1} (stretching band of aromatic CH).

The IR spectra of B-PNPs demonstrated characteristic bands of some functional groups, associated with the polymer (Fig. 2**e**). They showed some noticeable and prominent bands at 1088.15 cm^{-1} and 1171.45 cm^{-1} (for C–H bending vibrations), 1388.02 cm^{-1} (C = O bending vibration, not a prominent band), 1557.33 cm^{-1} (C = O stretching, small band), 1643.72 cm^{-1} (C–NH stretching, very small), 1753.17 cm^{-1} (C = O bending vibration, 2951.63 cm^{-1} (stretching band of aliphatic CH, depressed band), and 3335.08 cm^{-1} (stretching band of aromatic CH, slightly depressed band).

The IR spectra of SP-PNPs demonstrated characteristic bands of functional groups associated with the drugs and PLGA (Fig. 2**f**). They showed C–H bending vibrations at 683.34 cm^{-1} and 839.32 cm^{-1} (out of plane) and at 925.70 cm^{-1} (C–O stretching, likely of PIP), 1094.05 cm^{-1} (for C–H bending vibrations), 1128.44 cm^{-1} (C–O stretching), 1172.60 cm^{-1} (for C–H bending vibrations), 1558.47 cm^{-1} (C = O stretching band), 1641.22 cm^{-1} (C–NH stretching band), 1757.28 cm^{-1} (strong C = O bending vibration), 2946.83 cm^{-1}, 3298.18 cm^{-1} (stretching band of aliphatic CH), and 3335.15 cm^{-1} (stretching band of aromatic CH, slightly depressed band).

3.6. XRD analysis

XRD is a rapid and non-destructive analytical technique, mainly used for phase identification of crystalline substances and analysis of material microstructure. It works by irradiating samples with incident X-rays and measuring the scattering angles and intensities of the X-rays scattered by the samples (Ermrich and Opper, 2013). Graphs showing the relationship between the intensity of the scattered X-rays and scattering angle are plotted in Fig. 3. Chemical structures can be determined by analyzing the location in 2θ° angle and the intensities of the scattered intensity peaks. The X-ray diffractograms of the pure drugs (SORA and PIP), pure PLGA, the physical mixture of SORA, PIP, and PLGA, freeze-dried B-PNPs, and SP-PNPs are presented in Fig. 3.

The diffractogram of pure-SORA (Fig. 3**a**) showed intense peaks at 2θ of 11.58°, 18.78°, 22.64°, 23.08°, 24.94°, 25.38°, and 38.06° with d-values (Bragg's spacing) of 7.6354, 4.7212, 3.9242, 3.8504, 3.5673, 3.5064, and 2.3624, respectively. The intensities of 894 cps (I/I_0 34), 1031 cps (I/I_0 39), 857 cps (I/I_0 32), 663 cps (I/I_0 25), 2687 cps (I/I_0 100), 665 cps (I/I_0 25), and 682 cps (I/I_0 26) indicate a crystalline state to SORA (Ebadi et al., 2020).

The diffractogram of pure-PIP (Fig. 3**b**) showed intense peaks at 2θ angles of 14.2°, 14.86°, 19.68°, 21.46°, 22.42°, 22.66°, 25.78°, 25.92°, and 38.04°, corresponding to Bragg's spacings of 6.232, 5.9566, 4.5073, 4.1373, 3.9622, 3.9208, 3.4529, 3.4346, and 2.3636, respectively. The intensities of 3607 cps (I/I_0 47), 7815 cps (I/I_0 100), 2676 cps (I/I_0 35), 2871 cps (I/I_0 37), 6142 cps (I/I_0 79), 4963 cps (I/I_0 64), 5132 cps (I/I_0 66), 7519 cps (I/I_0 97), and 2948 cps (I/I_0 38), also indicate a crystalline nature to pure PIP (Ramos et al., 2023). The diffractogram of pure-PLGA (Fig. 3**c**) revealed intense peaks at 2θ angles of 38.02° and 44.24° with Bragg's spacings of 2.3648 and 2.0456, respectively, along with intensities of 1536 cps (I/I_0 100) and 535 cps (I/I_0 35), indicating the characteristic of the PLGA polymer (Sun et al., 2015).

The diffractogram of the physical mixture of PLGA and drugs (Fig. 3**d**) showed intense peaks at 2θ angles of 15.08°, 25.98°, 38.04°,

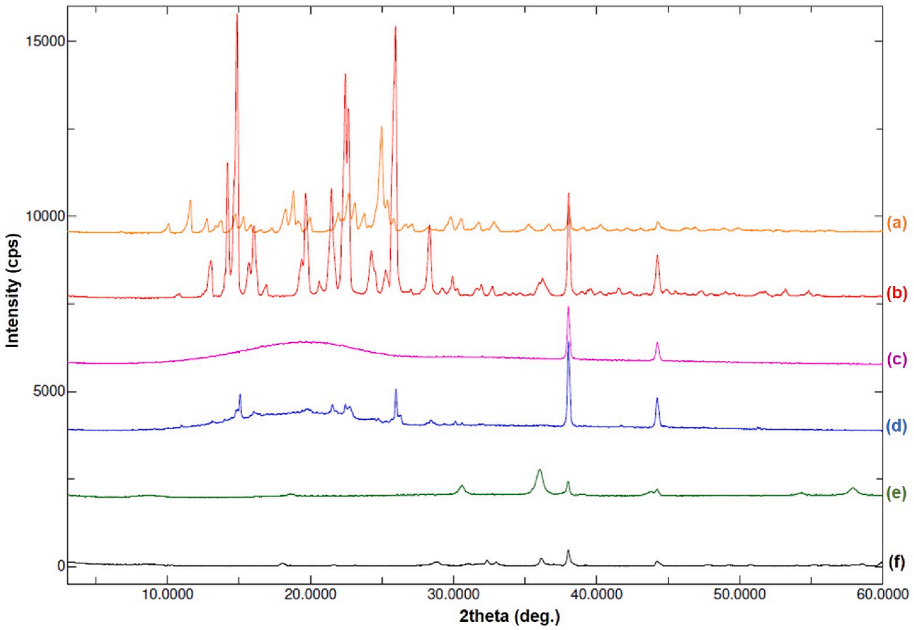

Fig. 3. Overlay diffractogram of pure-SORA **(a)**; pure-PIP **(b)**; pure-PLGA **(c)**; the physical mixture of drugs and PLGA **(d)**; B-PNPs **(e)**; SP-PNPs **(f)**.

and 44.24° with Bragg's spacings of 5.8702, 3.4268, 2.3636, and 2.0456, respectively, and intensities of 757 cps (I/I_0 33), 937 cps (I/I_0 40), 2353 cps (I/I_0 100), and 824 cps (I/I_0 36), indicating some of the intense and characteristic peaks of the pure drugs (SORA and PIP) and PLGA, which was expected because no changes in the molecular structure were observed in the physical mixture, and no interaction between PLGA and the drugs occurred.

The XRD-pattern of freeze-dried B-PNPs in Fig. 3**e** showed less intense diffraction peaks at 2θ angles of 30.58°, 36.0°, 38.0°, 44.42°, 57.9°, and 63.6° with d-values of 2.921, 2.4927, 2.366, 2.0465, 1.5913, and 1.4618, respectively, and intensities of 243 cps (I/I_0 40), 621 cps (I/I_0 100), 386 cps (I/I_0 63), 177 cps (I/I_0 29), 175 cps (I/I_0 29), and 191 cps (I/I_0 31). The diffraction peaks for B-PNPs appeared more or less (±0.5) around the 2θ angles of the polymer but with somewhat low intensities, suggesting low crystallinity of the polymer after passing through the different steps of formulation development. The diffraction patterns of freeze-dried SP-PNPs (Fig. 3**f**) showed intense peaks at 2θ angles of 28.84°, 32.36°, 36.12°, 38.02°, and 44.24° with Bragg's spacings of 3.0932, 2.7643, 2.4847, 2.3648, and 2.0456, respectively, and intensities of 100 cps (I/I_0 23), 123 cps (I/I_0 28), 200 cps (I/I_0 46), 443 cps (I/I_0 100), and 141 cps (I/I_0 32).

3.7. Drug release assessment

In vitro release profiling of drugs from nanoformulations can mimic their release behavior *in vivo*. Therefore, the *in vitro* release of SORA and PIP was assessed in this study using the conventional dialysis method. Drug release was investigated under two pH conditions, pH 7.4 (physiological pH) and pH 5 (mimicking solid tumor microenvironments). The concentrations of released drugs were estimated using HPLC-UV as described in Section 2.2. As shown in Fig. 4, the release of SORA and PIP from SP-PNPs at pH 5 and pH 7.4 was slower and sustained compared to the release of the pure drugs. At pH 5 (Fig. 4**a and 4b**), drug release from NPs was gradual and peaked at the 192-h time point (SORA: 77.7 ± 7.2 % and PIP: 61.3 ± 7.1 %), In contrast, the release of pure drugs was fast at the same pH, reaching nearly 92 % for SORA and 90 % for PIP at 12 h and 24 h, respectively.

As shown in Fig. 4**c and 4d,** at physiological pH, the cumulative release of SORA and PIP from SP-PNPs at the 192-h time point was 62.8 ± 6.4 % and 51.3 ± 2.4 %, respectively. Similarly, at pH 7.4, the release of SORA and PIP was also fast, reaching around 89 % and 87 % at 24 h, respectively. In both formulations (pure drugs and PLGA encapsulated), a higher release rate was observed in the slightly acidic environment (pH 5) compared to pH 7.4 which was expected (D'Souza, 2014) because SORA is more soluble at acidic pH (Park et al., 2020). In a previous study, a higher release rate of SORA was observed under acidic conditions (pH 4.7) from PEG and PVA-coated magnetic NPs compared to neutral pH (Ebadi et al., 2020).

The release kinetics of SORA and PIP from the SP-PNPs at pH 5 and pH 7.4 were investigated using various kinetic models including Zero-order, First-order, Korsmeyer-Peppas, Hixson-Crowell, and Higuchi-Matrix models. Results suggested sustained drug release characteristics of the developed PNPs **(Fig. S2 and S3)**. At pH 5, the results showed that the release of SORA from SP-PNPs was best fitted with Korsmeyer-Peppas model followed by the Higuchi-Matrix model (second-best model) with the highest coefficients of correlation (R^2 = 0.9982 and 0.9956, respectively). The release of PIP at pH 5 was best fitted with Hixson-Crowell model followed by the zero-order model with the highest R^2 values (0.9965 and 0.9933, respectively). At pH 7.4, the release of SORA was best fitted with the zero-order model followed by Hixson-Crowell model with the highest coefficients of correlation (R^2 = 0.9993 and 0.9958, respectively), whereas the release of PIP was best fitted with the Hixson-Crowell model followed by the zero-order model with the highest R^2 values (0.9926 and 0.9921, respectively).

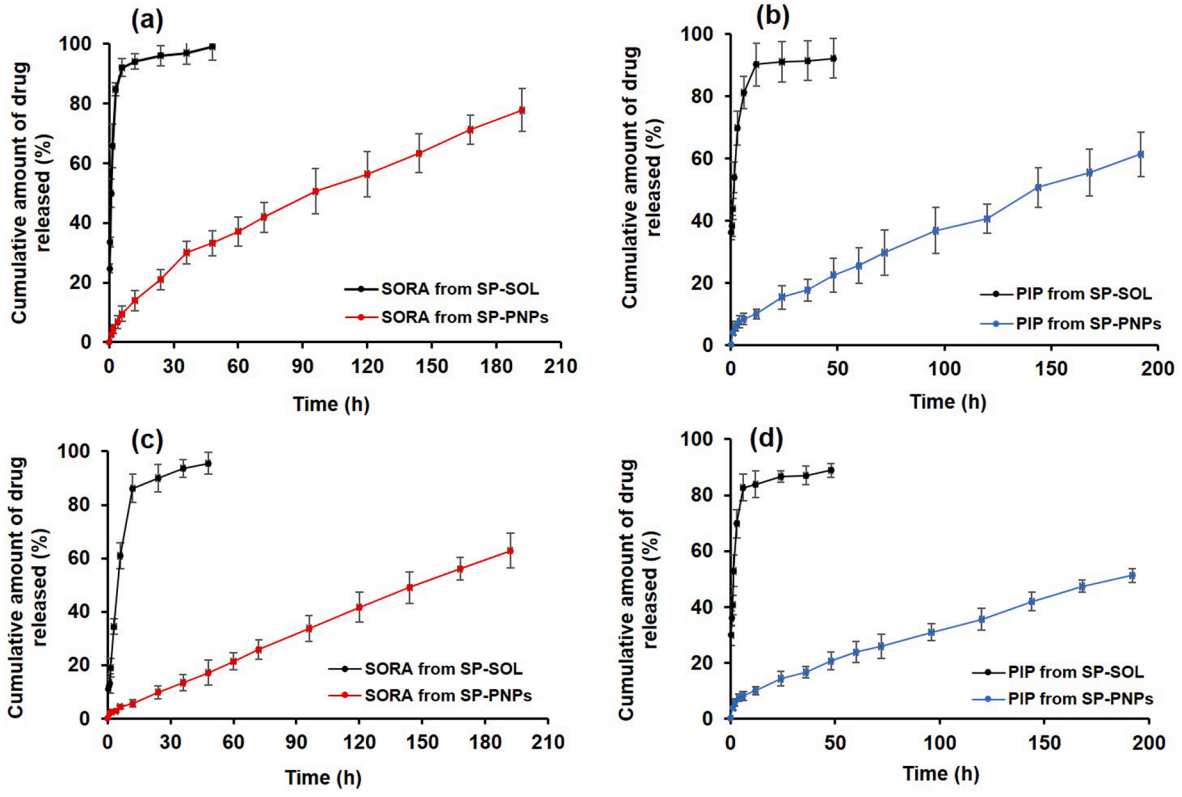

Fig. 4. Release profile of the pure drugs and PLGA-entrapped drugs in PBS, supplemented with 0.5 % Tween-80 at pH 5 and 7.4. SORA (pH 5) **(a)**; PIP (pH 5**) (b)**; SORA (pH 7.4) **(c)**; PIP (pH 7.4) **(d)**. All experiments were performed at 37 ± 0.5 °C and the data are presented as the means of three measurements with standard deviations (Mean ± SD, n = 3). PBS (phosphate buffered saline); SORA (Sorafenib); PIP (Piperine); SP-PNPs (SORA and PIP-loaded PLGA nanoparticles; SP-SOL (SORA and PIP dissolved in ethanol: Kolliphor® EL at 3: 1 v/v).

The linearity observed in the best-fitted models further suggested a sustained release property of SP-PNPs for both drugs. Given the slopes of the best fitted models, the diffusion-exponents (*n*-values) were calculated, and the numerical values of release constants were estimated. The R^2 values, slopes, K-values (release constant) and *n*-values (release/diffusion-exponents) of the different applied models are summarized in Table 3.

3.8. Cell proliferation study

To assess the impact of the developed dual anti-cancer therapy on HCC, MTT assay was performed on treated HepG2 cells (Fig. 5 and **Fig. S4)**. After 72 h of treatment, both single therapeutics (SORA and PIP as pure drugs) reduced cell viability and showed similar effects, with IC_{50} values of 7 and 8.2, respectively (Fig. 5**a)**. Dual therapy (SP-PNPs) significantly reduced cancer cell viability and showed superiority over single treatments (Fig. 5**a and 5b)** at a concentration range equivalent to SORA and half of PIP. The IC_{50} value for the SP-PNPs group was very low (0.74). Treatment of cells with the mixture of pure drugs resulted in a similar effect as SP-PNPs (IC_{50}: 0.87, **Fig. S4)**. However**,** B-PNPs had only a minor impact on HepG2 cells, suggesting that the developed PNPs are likely tolerable at low concentrations and do not induce pronounced cellular cytotoxicity, consistent with many previous studies investigating the cytotoxicity of PNPs on various cancer cell lines using the MTT assay (Elhabak et al., 2020; Mukerjee and Vishwanatha, 2009; Taebpour et al., 2021). Differences in the cytotoxic effect among the treatment groups compared to the control (Fig. 5**b)** were more clearly observed at low concentrations. SP-PNPs significantly decreased cellular viability across the entire concentration range, whereas SORA and PIP monotherapies did not markedly affect viability when used at concentrations below 3.75 μg/mL. This suggests that PIP exhibited a synergistic effect on HepG2 cells when combined with SORA. These results indicate that our therapeutic approach is likely effective in treating HCC.

3.9. Assessment of apoptosis/necrosis

The efficacy of the novel formulation, SP-PNPs, against HepG2 cells was further investigated using an apoptosis/necrosis assay. Cells were treated with low doses of SORA (2 μg/mL) and PIP (1 μg/mL) as single therapies, B-PNPs, and dual SP-PNPs therapy at the same concentrations for 72 h before being stained with PI and Annexin and analyzed via flow-cytometry. The results showed that, although statistically insignificant, the percentage of necrotic cells (PI^+ cells) increased upon treatment with SP-PNPs (**Fig. S5**), whereas other therapeutics did not have a noticeable effect. Treatment with PIP (at 1 μg/mL) did not lead to apparent cell death, whereas SORA monotherapy reduced cellular proliferation compared to the control as evidenced by the percentage of apoptotic cells and cell viability (Fig. 6**b and 6c**). SP-PNPs therapy had greater impact on cells; it significantly induced apoptosis ($Annexin^+$ + $Annexin^+$ PI^+ cells), resulting in a marked decrease in cell viability (Fig. 6**b and 6c**). These findings demonstrate that HepG2 cells predominantly undergo apoptosis upon dual treatment with SP-PNPs, and also confirm MTT results in which SP-PNPs therapy resulted in a marked increase in HepG2 cytotoxicity compared to monotherapies and B-PNPs.

4. Discussion

The HPLC method adopted in this study gave highly reproducible profiles for the determination of SORA and PIP at 280 nm UV-detection. In addition, the specificity and selectivity of the method were confirmed by the representative chromatograms showing SORA at 6.29 min and PIP at 4.98 min (**Fig. S1**). Our calibration results revealed good linearity between peak areas and drug concentrations. One of the advantages of this HPLC method is that no dual UV absorbance is needed because both SORA and PIP were well detected at 280 nm, which is considered the isosbestic point for both drugs. “An isosbestic point in spectroscopy is a particular wavelength (nm) at which two (or more) chemical substances or species have the same absorptivity” (Kaspar, 2023; Tiwari et al., 2020).

In this study, SP-PNPs were prepared using the double emulsion solvent evaporation method (Kalam and Alshamsan, 2017; Kwon et al., 2001). The evaporation of the organic solvent during the preparation of PNPs is a critical step in preventing aggregation and amalgamation of the droplets (Pulingam et al., 2022). When the oil–water interface forms, the stabilizer (PVA) helps in reducing the energy of the system and decrease the interfacial tension, and thereby preventing amalgamation or coalescence of the developed PNPs (Alkholief et al., 2022; Kalam and Alshamsan, 2017; Murakami et al., 1997; Shin et al., 2010; Tian et al., 2022).

The amount of PLGA in the organic phase plays a significant role in

Table 3
Release kinetic models applied to the drug release data obtained from SP-PNPs at two pH conditions. The correlation coefficient (R^2), rate constant, and half-life were acquired by fitting various kinetic equations to the SORA and PIP release data.

Release kinetics of SORA and PIP from SP-PNPs at pH 5.0								
SORA at pH 5					PIP at pH 5			
Release models	R^2 value	Slope	*K*	*n*-value	R^2 value	Slope	*K*	*n*-value
Zero-order	0.9670	0.0038	0.0110	0.0017	0.9933	0.0029	0.0112	0.0014
First-order	0.9919	0.0031	0.7482	0.0013	0.9932	0.0020	0.7486	0.0008
Korsmeyer-Peppas	0.9982	0.6304	0.2543	0.2737 **(FD)***	0.9751	0.5093	0.1886	0.2211
Hixson-Crowell	0.9930	0.0019	1.4029	0.0008	0.9965	0.0013	1.0802	0.0006 **(FD)***
Higuchi- Matrix	0.9956	0.0575	0.0435	0.0250	0.9690	0.0430	0.0354	0.0187
Release kinetics of SORA and PIP from SP-PNPs at pH 7.4								
SORA at pH 7.4					PIP at pH 7.4			
Release models	R^2 value	Slope	*K*	*n*-value	R^2 value	Slope	*K*	*n*-value
Zero-order	0.9993	0.0032	0.0063	0.0014 **(FD)***	0.9921	0.0207	0.0106	0.0089
First-order	0.9887	0.0021	0.7539	0.0009	0.9887	0.0379	0.7492	0.0165
Korsmeyer-Peppas	0.9687	0.6918	0.1566	0.3004	0.9779	0.3639	0.1683	0.1580
Hixson-Crowell	0.9958	0.0014	1.4012	0.0006	0.9926	0.0349	1.0800	0.015154 **(FD)***
Higuchi-Matrix	0.9494	0.0466	0.0251	0.0202	0.9678	0.1758	0.0326	0.076335

SORA = Sorafenib; PIP = Piperine; R^2 = Correlation coefficients; *K* = Release constant; *n*-value = Diffusion-exponent; and FD* = Fickian Diffusion

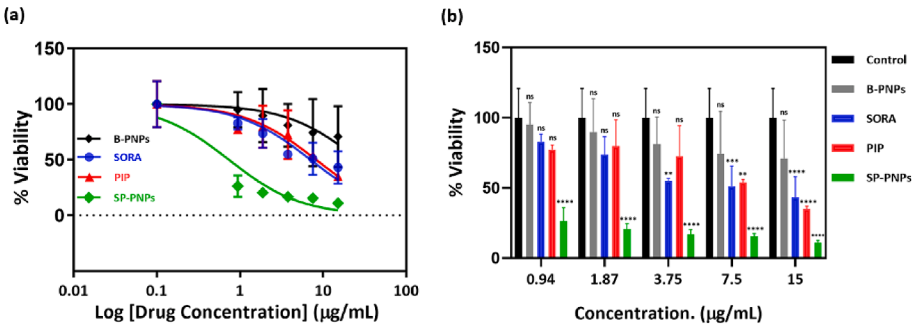

Fig. 5. Evaluation of the cytotoxicity of therapeutics toward HepG2 *in vitro* via MTT assay. The cytotoxicity curve was obtained after incubation of HepG2 cells for 72 h with B-PNPs, pure SORA (SORA), pure PIP (PIP), and SP-PNPs. IC_{50} values were calculated utilizing non-linear regression, log (inhibitor) *vs.* normalized response **(a)**; % cellular viability in response to the various treatments **(b)**. Statistical significance was calculated by comparing treatment groups with the control using ordinary One-way ANOVA test (**$p < 0.01$, ***$p < 0.001$, ****$p < 0.0001$). Data are represented as mean ± SD, $n = 4$.

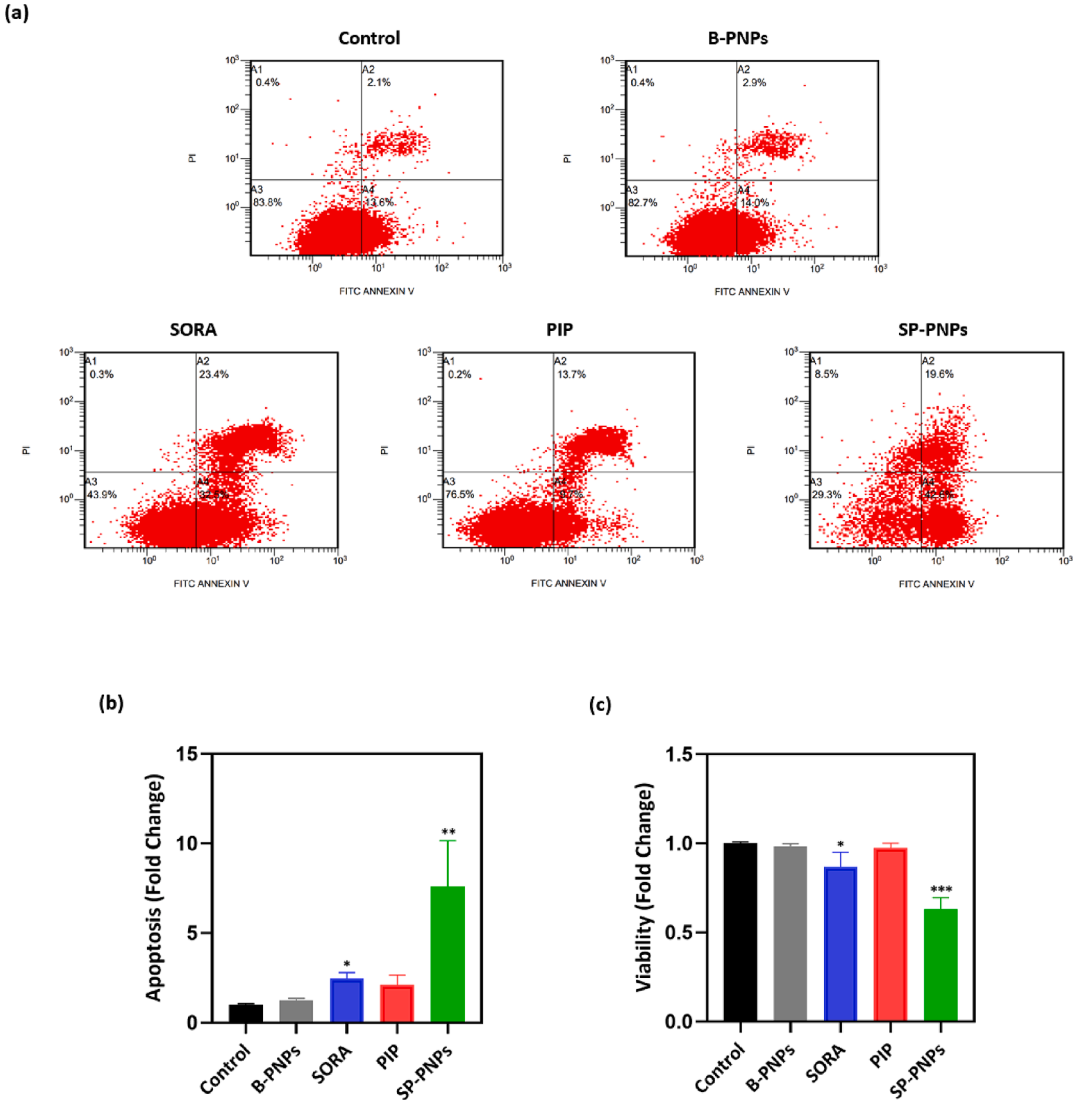

Fig. 6. Assessment of HepG2 apoptosis/necrosis after 72 h of treatment with B-PNPs, pure SORA (SORA), pure PIP (PIP), and SP-PNPs. Gating strategy on flow-cytometry **(a)**; Change in apoptosis ($Annexin^+$ + $Annexin^+$ PI^+) **(b)**; Change in viability ($Annexin^-$ PI^-) **(c)**. All samples were normalized to the average control in each independent experiment. Statistical significance was estimated by comparing treatment groups with the control using the Kruskal-Wallis test (*$p < 0.05$). Data are represented as mean ± SEM, $n = 6$.

the size of PLGA- based NPs (Chatterjee and Chanda, 2022). Our previous studies have shown higher amounts of PLGA in the organic phase result in larger PNPs (Alshamsan et al., 2020; Kalam and Alshamsan, 2017). Therefore, in the present work, the drug:polymer ratio used was ~ 1:9. The direct proportional relationship between PNPs size and the amount of PVA may be attributed to the strong bonding and close

association of the lipophilic part of PVA with the polymeric matrix (Prabha and Labhasetwar, 2004). Moreover, the mechanistic influence of PVA as a stabilizer on particle size can also be attributed to the interpenetration of PVA and PLGA fragments during PNPs formation. Based on our previous experience in PLGA-NPs development, the stabilizer PVA was found to be superior to polyvinyl-pyrrolidone (PVP) in terms of physical characteristics, even at a lower concentration (Alkholief et al., 2022). The low values of PDI in all the PNPs indicate uniformly distributed NPs, consistent with previous studies (Mainardes and Evangelista, 2005; Turk et al., 2014).

The observed negative ζ in SP-PNPs was likely due to incomplete shielding of the negative surface of PLGA (presence of –COOH functional groups) and the presence of PVA, which imparts a weak negative surface charge to the PNPs (Inam et al., 2022). Despite the low negative ζ, PNPs were well stabilized by PVA through a steric hindrance mechanism (Alkholief et al., 2022; Cegnar et al., 2004).

The SEM analysis revealed preferred properties for the polymeric NPs developed in this study, which confirms the suitability and applicability of the chosen formulation factors. The smooth surface and discrete nature of PNPs across all concentrations of PVA were attributed to the strong emulsification (high hydrophilic-lipophilic balance [HLB] > 18) and surface stabilization properties of PVA (Sakhi et al., 2023). The presence of PVA at the interface of nano-droplets during the emulsification stage of formulation development may prevent droplet merging and potential NP aggregation by decreasing the overall free energy of the two phases (Garcia-Melero et al., 2022).

IR spectral analyses of the pure drugs, excipients, their physical mixture, B-PNPs, and SP-PNPs suggested that both drugs were compatible with the polymer and other excipients used to develop PNPs. The appearance of a band at 1750 cm^{-1} is attributed to stretching vibrations of the C = O ester bond which is prominent and abundant in the structure of PLGA. Its presence in the spectra of B-PNPs and SP-PNPs in association with drugs-related bands indicates their compatibility, as suggested in a previous report (Caputo et al., 2023). The appearance of bands of functional groups associated with the drugs in the formulations confirmed that the preparation steps of SP-PNPs did not alter the basic chemical structures of the drugs in the presence of the organic solvent and the stabilizer (PVA of high HLB value [> 18]), as seen in a previous study (Cortes et al., 2021).

The absence of high-intensity diffraction peaks for SORA and PIP in the XRD diffractogram of SP-PNPs suggests that the drugs were encapsulated in the PNP core, because the crystallinity of the drugs was reduced and converted to amorphous forms, similar to what was seen in the encapsulation of SORA into PVA/LDH-and PEG/LDH-coated iron oxide NPs (Ebadi et al., 2020) and PIP encapsulation into solid lipid NPs (Bhalekar et al., 2017).The appearance of very small and low intensity peaks of PIP observed in the SP-PNP diffractogram (Fig. 3**f**) can be attributed to the presence of surface adsorbed PIP on the polymeric NPs. This finding can be correlated with the lower %EE of PIP compared to SORA.

The majority of FDA-approved anticancer therapeutics are developed as rapidly bioavailable dosage forms and, thus, they typically induce their activity in a short period of time. They are also cleared relatively quickly, so they usually require more frequent dosing. On the other hand, slowly released therapeutics maintain their levels in the body for a relatively longer time, allowing for continuous exposure. Many nanoformulations are tailored to allow for slow drug release (Adepu and Ramakrishna, 2021). Such characteristic is particularly important for anticancer drugs because patients usually use several medicines, some of which may require hospital visits (Pacheco et al., 2023). It has been shown that SORA exhibits slow-release profiles when incorporated into lipid-based nanoformulations (Yang et al., 2016; Zhang et al., 2012).

In our work, the sustained release of SORA and PIP from the PLGA matrix (in SP-PNPs) more likely occurred due to the following mechanisms: liberation/release of the drug(s) due to the degradation/erosion of the polymeric matrix, diffusion of the drug(s) from the matrix into the release medium, as well as a combination of these two mechanisms (Alkholief et al., 2022; Kalam and Alshamsan, 2017; Ritger and Peppas, 1987). These phenomena might have controlled the release of SORA and PIP up to 192 h.

The calculated values of the diffusion-exponents (<0.5) for the best-fitted models indicate that the released drugs followed a Fickian-Diffusion type of release mechanism, as suggested in previous reports (Chime et al., 2013; Guo et al., 2023; Ritger and Peppas, 1987; Unagolla and Jayasuriya, 2018).

The anti-cancer efficacy of dual SORA and PIP therapy on liver and breast cancers was previously evaluated (Mohany et al., 2021). El-Shehawy et al. conducted a study employing a therapeutic combination strategy, in which Thymoquinone and PIP were combined with SORA for the treatment of liver and breast malignancies. *In vitro* studies, including MTT assay, revealed that the combination therapeutic approach was more cytotoxic compared to each single treatment (El-Shehawy et al., 2023). However, the lipophilic drugs were dissolved in human incompatible solvents, unlike in this present study, where a translatable, biocompatible FDA-approved vehicle (PLGA) was used. Another study has investigated the effect of SORA and PIP combination therapy on triple negative breast cancer *in vitro*, showing its enhanced effectiveness against breast cancer cells compared to each drug alone; however, the vehicles used were also not intended for human use (Mohany et al., 2021). Nevertheless, those studies provided a proof of concept for utilizing SORA and PIP as a dual therapeutic, which in this work was highly effective.

PIP is a pleiotropic natural compound. In the context of cancer, besides its direct antitumor activity, PIP has been shown to enhance the efficacy of anti-malignant drugs by inhibiting the drug-metabolizing enzyme CYP3A4 and by reducing drug resistance through its effect of blunting Pgp efflux transporter (Benayad et al., 2023; Gao and Hu, 2010). In this study, the marked effect of SP-PNPs compared to pure SORA on HepG2 cells was likely because PIP synergistically enhanced the cytotoxic effect on HepG2 cells, which was also seen in previous studies where PIP was used in combination with chemotherapeutics (Fattah et al., 2021; Pal et al., 2016). Taken together, efficacy studies highlight the benefits of using PIP as an add-on therapy to the standard of care SORA for the treatment of HCC.

This work demonstrates the potential of PIP to support SORA synergistically when formulated in PNPs to treat liver cancer. Future studies will focus on *in vivo* investigation of this novel strategy, including drug escalation studies, and extensive safety and efficacy studies conducted using a murine cancer model.

5. Conclusions

In this study, SORA and PIP were successfully loaded into PLGA NPs using the emulsification-solvent-evaporation method. Results showed that the candidate formulation (SP-PNPs with 0.5 % PVA) was spherical in shape with no obvious aggregation of particles, approximately 225 nm in size with low PDI (0.131) and small negative ζ (−5.01 mV), and exhibited a high %EE (SORA: ~82 %, PIP: ~79 %). Moreover, drugs entrapped in such nano-carriers were in an amorphous state and their release pattern *in vitro* was sustained in both physiological and acidic pH environments. At pH 7.4, 62.8 % of SORA and 51.3 % of PIP were released over 192 h, whereas at pH 5, 77.7 % of SORA and 61.3 % of PIP were released. The release behavior of the drugs was also assessed using kinetic models, which showed that Fickian-diffusion was the mechanism of drug release. Cell proliferation study and apoptosis analysis revealed that PLGA-encapsulated SORA and PIP, as a dual therapy, was more effective than SORA monotherapy in killing HepG2 cells. These results indicate that SP-PNPs may potentially be an efficient treatment strategy for the management of HCC and may offer an opportunity for further investigation through pre-clinical and clinical studies. Our future research will be directed toward *in vivo* safety and efficacy assessment of

SP-PNPs using an appropriate mouse HCC model.

CRediT authorship contribution statement

Sulaiman S. Alhudaithi: Conceptualization, Data curation, Formal analysis, Funding acquisition, Investigation, Methodology, Project administration, Supervision, Validation, Writing – original draft, Writing – review & editing. **Mohd Abul Kalam:** Data curation, Formal analysis, Methodology, Writing – original draft. **Lama Binobaid:** Data curation, Investigation, Methodology. **Raisuddin Ali:** Data curation, Formal analysis, Methodology. **Mohammed M. Almutairi:** Data curation, Investigation, Methodology. **Wajhul Qamar:** Data curation, Investigation, Methodology. **Hessa Bin Hithlayn:** Data curation, Investigation, Methodology. **Atheer Almutairi:** Data curation, Investigation, Methodology. **Abdullah K. Alshememry:** Investigation, Validation, Writing – review & editing.

Declaration of competing interest

The authors declare that they have no known competing financial interests or personal relationships that could have appeared to influence the work reported in this paper.

Acknowledgments

This work was supported by Researchers Supporting Project number (RSPD2024R598), King Saud University, Riyadh, Saudi Arabia.

Appendix A. Supplementary data

Supplementary data to this article can be found online at https://doi.org/10.1016/j.jsps.2024.102064.

References

Adepu, S., Ramakrishna, S., 2021. Controlled drug delivery systems: current status and future directions. Molecules 26, 5905.
Alkholief, M., Kalam, M.A., Anwer, M.K., Alshamsan, A., 2022. Effect of solvents, stabilizers and the concentration of stabilizers on the physical properties of poly (D, L-lactide-co-glycolide) nanoparticles: encapsulation, in vitro release of indomethacin and cytotoxicity against HepG2-cell. Pharmaceutics 14, 870.
Alsaab, H.O., Alharbi, F.D., Alhibs, A.S., Alanazi, N.B., Alshehri, B.Y., Saleh, M.A., Alshehri, F.S., Algarni, M.A., Almugaiteeb, T., Uddin, M.N., Alzhrani, R.M., 2022. PLGA-based nanomedicine: history of advancement and development in clinical applications of multiple diseases. Pharmaceutics 14.
Alshamsan, A., Binkhathlan, Z., Kalam, M.A., Qamar, W., Kfouri, H., Alghonaim, M., Lavasanifar, A., 2020. Mitigation of tacrolimus-associated nephrotoxicity by PLGA Nanoparticulate delivery following multiple dosing to mice while maintaining its immunosuppressive activity. Sci Rep 10, 6675.
Alvi, M., Yaqoob, A., Rehman, K., Shoaib, S.M., Akash, M.S.H., 2022. PLGA-based nanoparticles for the treatment of cancer: current strategies and perspectives. AAPS Open 8, 12.
Bai, X., Smith, Z.L., Wang, Y., Butterworth, S., Tirella, A., 2022. Sustained Drug Release from Smart Nanoparticles in Cancer Therapy: A Comprehensive Review. Micromachines (Basel) 13.
Ben Mousa, A., 2008. Sorafenib in the treatment of advanced hepatocellular carcinoma. Saudi J Gastroenterol 14, 40–42.
Benayad, S., Wahnou, H., El Kebbaj, R., Liagre, B., Sol, V., Oudghiri, M., Saad, E.M., Duval, R.E., Limami, Y., 2023. The Promise of Piperine in Cancer Chemoprevention. Cancers (Basel) 15.
Bhalekar, M.R., Madgulkar, A.R., Desale, P.S., Marium, G., 2017. Formulation of piperine solid lipid nanoparticles (SLN) for treatment of rheumatoid arthritis. Drug Dev Ind Pharm 43, 1003–1010.
Caputo, T.M., Cusano, A.M., Principe, S., Cicatiello, P., Celetti, G., Aliberti, A., Micco, A., Ruvo, M., Tagliamonte, M., Ragone, C., Minopoli, M., Carriero, M.V., Buonaguro, L., Cusano, A., 2023. Sorafenib-loaded PLGA Carriers for enhanced drug delivery and Cellular uptake in liver cancer cells. Int J Nanomedicine 18, 4121–4142.
Cegnar, M., Kos, J., Kristl, J., 2004. Cystatin incorporated in poly(lactide-co-glycolide) nanoparticles: development and fundamental studies on preservation of its activity. Eur. J. Pharm. Sci. 22, 357–364.
Chatterjee, M., Chanda, N.J.M.A., 2022. Formulation of PLGA Nano-Carriers: Specialized Modification for Cancer Therapeutic Applications. 3, 837–858.
Chime, S., Onunkwo, G., Onyishi, I., 2013. Kinetics and mechanisms of drug release from swellable and non swellable matrices: a review. Res J Pharm Biol Chem Sci 4, 97–103.
Colagrande, S., Inghilesi, A.L., Aburas, S., Taliani, G.G., Nardi, C., Marra, F., 2016. Challenges of advanced hepatocellular carcinoma. World J Gastroenterol 22, 7645–7659.
Cortes, H., Hernandez-Parra, H., Bernal-Chavez, S.A., Prado-Audelo, M.L.D., Caballero-Floran, I.H., Borbolla-Jimenez, F.V., Gonzalez-Torres, M., Magana, J.J., Leyva-Gomez, G., 2021. Non-Ionic Surfactants for stabilization of Polymeric Nanoparticles for biomedical uses. Materials (basel) 14.
D'Souza, S., 2014. A review ofIn VitroDrug release test methods for Nano-sized dosage forms. Advances in Pharmaceutics 2014, 1–12.
Ebadi, M., Bullo, S., Buskara, K., Hussein, M.Z., Fakurazi, S., Pastorin, G., 2020. Release of a liver anticancer drug, sorafenib from its PVA/LDH-and PEG/LDH-coated iron oxide nanoparticles for drug delivery applications. Sci. Rep. 10, 21521.
Eid, M.M., 2022. Characterization of Nanoparticles by FTIR and FTIR-microscopy. Handbook of Consumer Nanoproducts. Springer 1–30.
Elhabak, M., Osman, R., Mohamed, M., El-Borady, O.M., Awad, G.A.S., Mortada, N., 2020. Near IR responsive targeted integrated lipid polymer nanoconstruct for enhanced magnolol cytotoxicity in breast cancer. Sci. Rep. 10, 8771.
El-Shehawy, A.A., Elmetwalli, A., El-Far, A.H., Mosallam, S.-A.-E.-R., Salama, A.F., Babalghith, A.O., Mahmoud, M.A., Mohany, H., Gaber, M., El-Sewedy, T., 2023. Thymoquinone, piperine, and sorafenib combinations attenuate liver and breast cancers progression: epigenetic and molecular docking approaches. BMC Complementary Medicine and Therapies 23, 1–21.
Ermrich, M., Opper, D., 2013. XRD for the analyst. Getting acquainted with the principles. Second, Panalytical.
Escudero-Ortiz, V., Pérez-Ruixo, J.J., Valenzuela, B., 2015. Development and validation of an HPLC-UV method for pazopanib quantification in human plasma and application to patients with cancer in routine clinical practice. Therapeutic Drug Monitoring 37, 172–179.
Fattah, A., Morovati, A., Niknam, Z., Mashouri, L., Asadi, A., Rizi, S.T., Abbasi, M., Shakeri, F., Abazari, O., 2021. The synergistic combination of cisplatin and piperine induces apoptosis in MCF-7 cell line. Iran. J. Public Health 50, 1037.
Finch, A., Pillans, P., 2014. P-glycoprotein and its role in drug-drug interactions. Aust. Prescr. 37.
Furuse, J., 2008. Sorafenib for the treatment of unresectable hepatocellular carcinoma. Biologics 2, 779–788.
Gao, S., Hu, M., 2010. Bioavailability challenges associated with development of anti-cancer phenolics. Mini Rev Med Chem 10, 550–567.
Garcia-Melero, J., Lopez-Mitjavila, J.J., Garcia-Celma, M.J., Rodriguez-Abreu, C., Grijalvo, S., 2022. Rosmarinic Acid-Loaded Polymeric Nanoparticles Prepared by Low-Energy Nano-Emulsion Templating: Formulation, Biophysical Characterization, and In Vitro Studies. Materials (Basel) 15.
Gomaa, A.I., Khan, S.A., Toledano, M.B., Waked, I., Taylor-Robinson, S.D., 2008. Hepatocellular carcinoma: epidemiology, risk factors and pathogenesis. World J Gastroenterol 14, 4300–4308.
Guo, Y., Li, X., Macgregor, R.B., Yan, H., Zhang, R.X., 2023. Microfluidics-based PLGA nanoparticles of ratiometric multidrug: from encapsulation and release rates to cytotoxicity in human lens epithelial cells. Heliyon 9, e18318.
Inam, W., Bhadane, R., Akpolat, R.N., Taiseer, R.A., Filippov, S.K., Salo-Ahen, O.M., Rosenholm, J.M., Zhang, H.J.V., 2022. Interactions between Polymeric Nanoparticles and Different Buffers as Investigated by Zeta Potential Measurements and Molecular Dynamics Simulations. 3, 20210009.
Kalam, M.A., Alshamsan, A., 2017. Poly (d, l-lactide-co-glycolide) nanoparticles for sustained release of tacrolimus in rabbit eyes. Biomed. Pharmacother. 94, 402–411.
Kaspar, F., 2023. Quality data from messy spectra: how isometric points increase information content in highly overlapping spectra. Chembiochem 24, e202200744.
Kopustinskiene, D.M., Jakstas, V., Savickas, A., Bernatoniene, J., 2020. Flavonoids as anticancer agents. Nutrients 12.
Kwon, H.-Y., Lee, J.-Y., Choi, S.-W., Jang, Y., Kim, J.-H., 2001. Preparation of PLGA nanoparticles containing estrogen by emulsification–diffusion method. Colloids Surf A Physicochem Eng Asp 182, 123–130.
Laface, C., Fedele, P., Maselli, F.M., Ambrogio, F., Foti, C., Molinari, P., Ammendola, M., Lioce, M., Ranieri, G., 2022. Targeted Therapy for Hepatocellular Carcinoma: Old and New Opportunities. Cancers (Basel) 14.
Li, B., Shao, H., Gao, L., Li, H., Sheng, H., Zhu, L., 2022. Nano-drug co-delivery system of natural active ingredients and chemotherapy drugs for cancer treatment: a review. Drug Deliv 29, 2130–2161.
Liu, C., Chen, Z., Chen, Y., Lu, J., Li, Y., Wang, S., Wu, G., Qian, F., 2016. Improving oral bioavailability of sorafenib by optimizing the "spring" and "parachute" based on molecular interaction mechanisms. Mol. Pharm. 13, 599–608.
Lu, Y., Cheng, D., Niu, B., Wang, X., Wu, X., Wang, A., 2023. Properties of Poly (Lactic-co-Glycolic Acid) and Progress of Poly (Lactic-co-Glycolic Acid)-Based Biodegradable Materials in Biomedical Research. Pharmaceuticals (Basel) 16.
Mainardes, R.M., Evangelista, R.C., 2005. PLGA nanoparticles containing praziquantel: effect of formulation variables on size distribution. Int J Pharm 290, 137–144.
Makadia, H.K., Siegel, S.J., 2011. Poly lactic-co-glycolic acid (PLGA) as biodegradable controlled drug delivery Carrier. Polymers (basel) 3, 1377–1397.
Mohany, H., Mahmoud, M.A., El-Shehawy, A.A., Gaber, M., Elmetwalli, A., Salama, A.F., El Sewedy, T., 2021. Antioxidant and cytotoxicity potential of Piperine and sorafenib combination in human MDA-MB-231 breast cancer cells. Biochemistry Letters 17, 108–116.
Mukerjee, A., Vishwanatha, J.K., 2009. Formulation, characterization and evaluation of curcumin-loaded PLGA nanospheres for cancer therapy. Anticancer Res 29, 3867–3875.
Murakami, H., Kawashima, Y., Niwa, T., Hino, T., Takeuchi, H., Kobayashi, M., 1997. Influence of the degrees of hydrolyzation and polymerization of poly (vinylalcohol)

on the preparation and properties of poly (DL-lactide-co-glycolide) nanoparticle. Int. J. Pharm. 149, 43–49.
Neureiter, D., Stintzing, S., Kiesslich, T., Ocker, M., 2019. Hepatocellular carcinoma: therapeutic advances in signaling, epigenetic and immune targets. World J Gastroenterol 25, 3136–3150.
Nguyen, D.T., Nguyen, D.H., Nguyen, V.T.H., 2023. Sorafenib as first-line treatment for patients with primary hepatocellular carcinoma: an outcome evaluation. J Int Med Res 51, 3000605231179928.
Pacheco, C., Baiao, A., Ding, T., Cui, W., Sarmento, B., 2023. Recent advances in long-acting drug delivery systems for anticancer drug. Adv. Drug Deliv. Rev. 114724.
Pal, M.K., Jaiswar, S.P., Srivastav, A.K., Goyal, S., Dwivedi, A., Verma, A., Singh, J., Pathak, A.K., Sankhwar, P.L., Ray, R.S., 2016. Synergistic effect of piperine and paclitaxel on cell fate via cyt-c, Bax/Bcl-2-caspase-3 pathway in ovarian adenocarcinomas SKOV-3 cells. Eur J Pharmacol 791, 751–762.
Park, J.-H., Baek, M.-J., Lee, J.-Y., Kim, K.-T., Cho, H.-J., Kim, D.-D., 2020. Preparation and characterization of sorafenib-loaded microprecipitated bulk powder for enhancing oral bioavailability. Int. J. Pharm. 589, 119836.
Patel, K.A., Bhatt, M.H., Hirani, R.V., Patel, V.A., Patel, V.N., Shah, G.B., Chorawala, M. R., 2022. Assessment of potential drug-drug interactions among outpatients in a tertiary care hospital: focusing on the role of P-glycoprotein and CYP3A4 (retrospective observational study). Heliyon 8, e11278.
Prabha, S., Labhasetwar, V., 2004. Critical determinants in PLGA/PLA nanoparticle-mediated gene expression. Pharm Res 21, 354–364.
Pulingam, T., Foroozandeh, P., Chuah, J.A., Sudesh, K., 2022. Exploring Various Techniques for the Chemical and Biological Synthesis of Polymeric Nanoparticles. Nanomaterials (Basel) 12.
Ramos, I.N.F., da Silva, M.F., Lopes, J.M.S., Cruz, J.N., Alves, F.S., do Rego, J.A.R., Costa, M.L.D., Assumpcao, P.P., Barros Brasil, D.D.S., Khayat, A.S., 2023. Extraction, Characterization, and evaluation of the cytotoxic activity of Piperine in its isolated form and in combination with chemotherapeutics against gastric cancer. Molecules 28.
Rezvantalab, S., Drude, N.I., Moraveji, M.K., Güvener, N., Koons, E.K., Shi, Y., Lammers, T., Kiessling, F., 2018. PLGA-based nanoparticles in cancer treatment. Front. Pharmacol. 9, 1260.
Ritger, P.L., Peppas, N.A., 1987. A simple equation for description of solute release I. fickian and non-fickian release from non-swellable devices in the form of slabs, spheres, cylinders or discs. J. Control. Release 5, 23–36.
Rocha, C.V., Goncalves, V., da Silva, M.C., Banobre-Lopez, M., Gallo, J., 2022. PLGA-based composites for Various biomedical applications. Int J Mol Sci 23.
Sakhi, M., Khan, A., Khan, I., Ahmad Khan, S., Irum Khan, S., Ali Khattak, M., Uddin, M. N., Kazi, M., Nasir, F., 2023. Effect of polymeric stabilizers on the size and stability of PLGA paclitaxel nanoparticles. Saudi Pharm J 31, 101697.
Shao, L., Shen, S., Liu, H., 2022. Recent advances in PLGA micro/nanoparticle delivery systems as novel therapeutic approach for drug-resistant tuberculosis. Front Bioeng Biotechnol 10, 941077.
Shin, S.-B., Cho, H.-Y., Kim, D.-D., Choi, H.-G., Lee, Y.-B., 2010. Preparation and evaluation of tacrolimus-loaded nanoparticles for lymphatic delivery. Eur. J. Pharm. Biopharm. 74, 164–171.
Shoba, G., Joy, D., Joseph, T., Majeed, M., Rajendran, R., Srinivas, P.S., 1998. Influence of piperine on the pharmacokinetics of curcumin in animals and human volunteers. Planta Med 64, 353–356.
Siegel, R.L., Miller, K.D., Jemal, A., 2019. Cancer statistics, 2019. CA Cancer J Clin 69, 7–34.
Singh, G., Kaur, T., Kaur, R., Kaur, A., 2014. Recent biomedical applications and patents on biodegradable polymer-PLGA. Int. J. Pharmacol. Pharm. Sci 1, 30–42.
Song, X., Zhao, Y., Wu, W., Bi, Y., Cai, Z., Chen, Q., Li, Y., Hou, S., 2008. PLGA nanoparticles simultaneously loaded with vincristine sulfate and verapamil hydrochloride: systematic study of particle size and drug entrapment efficiency. Int. J. Pharm. 350, 320–329.
Stăncioiu, L., Gherman, A.M.R., Brezeștean, I., Dina, N.E., 2022. Vibrational spectral analysis of sorafenib and its molecular docking study compared to other TKIs. J. Mol. Struct. 1248, 131507.
Storandt, M.H., Mahipal, A., Tella, S.H., Kommalapati, A., Jin, Z., 2022. Systemic therapy in advanced Hepatocellular Carcinoma: patient selection and key considerations. J Hepatocell Carcinoma 9, 1187–1200.
Sun, S.B., Liu, P., Shao, F.M., Miao, Q.L., 2015. Formulation and evaluation of PLGA nanoparticles loaded capecitabine for prostate cancer. Int J Clin Exp Med 8, 19670–19681.
Syed, S.B., Arya, H., Fu, I.H., Yeh, T.K., Periyasamy, L., Hsieh, H.P., Coumar, M.S., 2017. Targeting P-glycoprotein: investigation of piperine analogs for overcoming drug resistance in cancer. Sci Rep 7, 7972.
Taebpour, M., Arasteh, F., Akhlaghi, M., Haghirosadat, B.F., Oroojalian, F., Tofighi, D., 2021. Fabrication and characterization of PLGA polymeric nanoparticles containing berberine and its cytotoxicity on breast cancer cell (MCF-7). Nanomedicine Research Journal 6, 396–408.
Tian, Y., Zhou, J., He, C., He, L., Li, X., Sui, H., 2022. The formation, stabilization and separation of oil–water emulsions: a review. Processes 10, 738.
Tiwari, A., Mahadik, K.R., Gabhe, S.Y., 2020. Effect of piperine and its analogs on pharmacokinetic properties of sorafenib tosylate: bioanalytical method development and validation. Journal of Applied Pharmaceutical Science 10, 001–012.
Tiwari, A., Modi, S.J., Gabhe, S.Y., Kulkarni, V.M., 2021. Evaluation of piperine against cancer stem cells (CSCs) of hepatocellular carcinoma: insights into epithelial-mesenchymal transition (EMT). Bioorg. Chem. 110, 104776.
Tripathi, A.K., Ray, A.K., Mishra, S.K., 2022. Molecular and pharmacological aspects of piperine as a potential molecule for disease prevention and management: evidence from clinical trials. Beni Suef Univ J Basic Appl Sci 11, 16.
Turk, C.T., Oz, U.C., Serim, T.M., Hascicek, C., 2014. Formulation and optimization of nonionic surfactants emulsified nimesulide-loaded PLGA-based nanoparticles by design of experiments. AAPS PharmSciTech 15, 161–176.
Unagolla, J.M., Jayasuriya, A.C., 2018. Drug transport mechanisms and in vitro release kinetics of vancomycin encapsulated chitosan-alginate polyelectrolyte microparticles as a controlled drug delivery system. Eur J Pharm Sci 114, 199–209.
Wang, Y.M., Lin, W., Chai, S.C., Wu, J., Ong, S.S., Schuetz, E.G., Chen, T., 2013. Piperine activates human pregnane X receptor to induce the expression of cytochrome P450 3A4 and multidrug resistance protein 1. Toxicol Appl Pharmacol 272, 96–107.
Yang, J.D., Hainaut, P., Gores, G.J., Amadou, A., Plymoth, A., Roberts, L.R., 2019. A global view of hepatocellular carcinoma: trends, risk, prevention and management. Nat Rev Gastroenterol Hepatol 16, 589–604.
Yang, Y., Xiong, L., Li, M., Jiang, P., Wang, J., Li, C., 2023. Advances in radiotherapy and immunity in hepatocellular carcinoma. J. Transl. Med. 21, 526.
Yang, S., Zhang, B., Gong, X., Wang, T., Liu, Y., Zhang, N., 2016. In vivo biodistribution, biocompatibility, and efficacy of sorafenib-loaded lipid-based nanosuspensions evaluated experimentally in cancer. Int J Nanomedicine 11, 2329–2343.
Zarai, Z., Boujelbene, E., Salem, N.B., Gargouri, Y., Sayari, A., 2013. Antioxidant and antimicrobial activities of various solvent extracts, piperine and piperic acid from Piper nigrum. Lwt-Food Science and Technology 50, 634–641.
Zhang, Y.L., Cui, X.J., Xing, H., Ning, H.F., Dong, P., Wang, G.Z., 2023. Molecular targeted therapy and immunotherapy in advanced hepatocellular carcinoma: a systematic review and bayesian network meta-analysis based on randomized controlled trials. Ann Med 55, 2242384.
Zhang, H., Zhang, F.M., Yan, S.J., 2012. Preparation, in vitro release, and pharmacokinetics in rabbits of lyophilized injection of sorafenib solid lipid nanoparticles. Int J Nanomedicine 7, 2901–2910.
Zhuo, Y., Chen, Q., Chhatwal, J., 2019. Changing Epidemiology of Hepatocellular Carcinoma and Role of Surveillance, in: Hoshida, Y. (Ed.), Hepatocellular Carcinoma: Translational Precision Medicine Approaches, Cham (CH), pp. 53-67.